Landmarks in Earth Reinforcement, Ochiai et al. (eds),
© 2001 Swets & Zeitlinger, ISBN 90 2651 863 3

Seismic earth pressures acting on reinforced-soil and conventional type retaining walls

Junichi Koseki
Institute of Industrial Science, University of Tokyo, Japan

Kenji Watanabe, Masaru Tateyama and Kenichi Kojima
Railway Technical Research Institute, Japan

ABSTRACT: Comparisons are made on the resultant force of normal earth pressures that were measured in a series of model tests on six different types of soil retaining walls with a height of 530 or 500 mm, backfilled with dense dry sand. They consist of three reinforced-soil retaining walls with a full-height rigid facing and three conventional (cantilever, gravity and leaning) type retaining walls. The resultant forces of normal earth pressures measured in tilting tests were, in a broad sense, comparable with theoretical ones based on the Mononobe-Okabe or its equivalent method. On the other hand, the resultant forces measured in sinusoidal and irregular shaking tests were smaller than those measured in the tilting tests. However, by making corrections for the horizontal and vertical response accelerations of soil wedge in the backfill, the measured values became much close to the theoretical ones, in particular, in the region at high seismic loads.

1 INTRODUCTION

In order to establish practical design procedures to evaluate seismic stability of different types of retaining walls (RWs) against high seismic loads, a series of shaking table tests with irregular wave were conducted by Watanabe et al. (2001) on RW models consisting of six different types. This series of tests followed the previous series of tilting tests and sinusoidal shaking tests conducted on the same types of RW models, as reported by Koseki et al. (1998a, 1999). In the present paper, comparisons are made on the resultant force of normal earth pressures that were measured in these model tests.

2 TEST PROCEDURES

2.1 *Model walls*

The cross-sections of RW models are shown in Fig. 2 of Watanabe et al. (2001). All the models were 600 mm in width. The cantilever type and gravity type RWs were 530 mm high with vertical back face and base footing width of 230 mm. The leaning type RW was also 530 mm high, while it had inclined back face and base footing width of 180 mm.

The three types of reinforced-soil RWs were 500 mm high with a full height rigid facing having different arrangements of reinforcement layers. For the reinforced-soil wall type 1, ten layers of reinforcement strips having a length of 200 mm were horizontally placed in the backfill sand at a vertical spacing of 50 mm. For the reinforced-soil wall type 2, the length of the top and fourth reinforcement layers was increased to 800 mm and 450 mm, respectively. The length of all the reinforcement layers was increased to 350 mm for the reinforced-soil wall type 3.

A grid of phosphor-bronze strips was used as the model reinforcement. To form a model grid reinforcement layer, strips having a thickness of 0.1mm and a width of 3 mm were soldered to each other at an interval of 50 mm in the longitudinal direction, in parallel with the side wall, and 100 mm in the transverse direction, in parallel with the facing, as shown in Fig. 1. To effectively mobilize friction between the reinforcement and the backfill, sand particles were glued on the surface of the strips. The details of the model wall and reinforcement configurations are described in Koseki et al. (1998a).

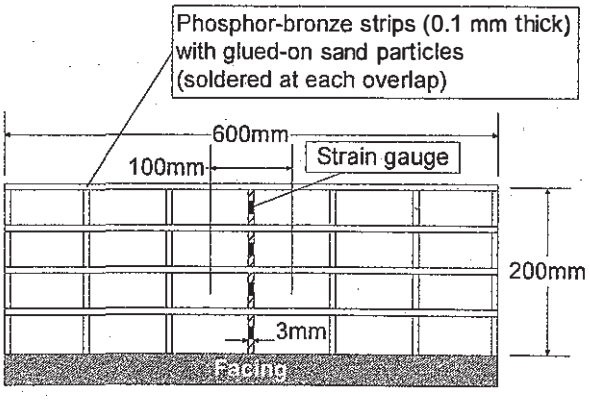

Figure 1. Plan of model grid reinforcement layer.

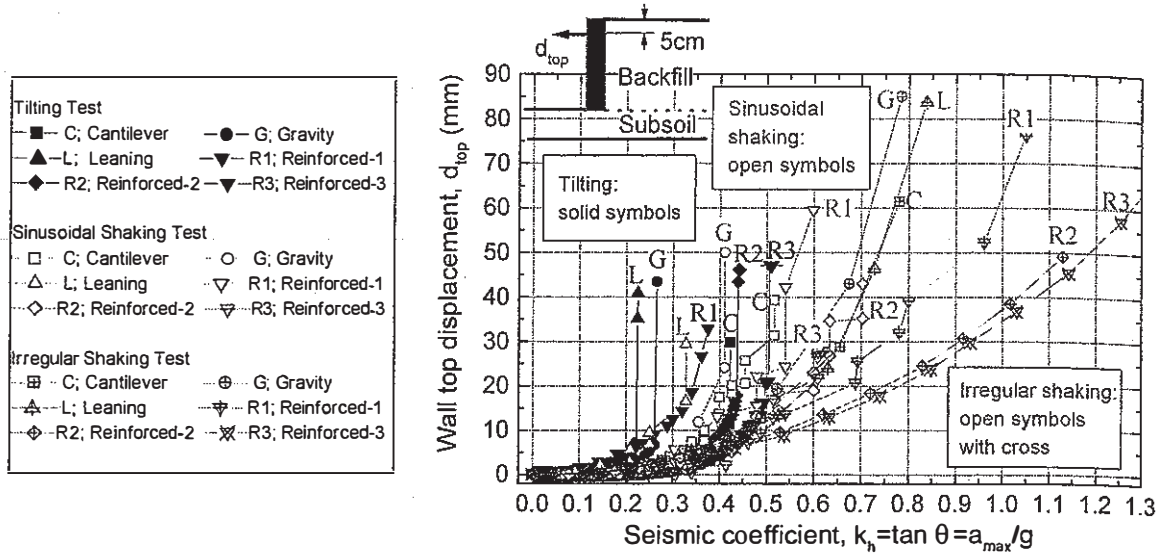

Figure 2. Accumulation of residual horizontal displacement near the top of the wall.

Shear load in the vertical direction and normal lateral load acting on the backface of wall were measured with a number of small two-component loadcells that were set on the back of wall along its center line, as shown in Fig. 3 of Watanabe et al. (2001). By using a piece of sponge covered by Teflon-sheet and smeared with silicone grease, the friction between the side of the wall and the side wall of the sand box was reduced, and the sealing between them was also achieved.

2.2 *Backfill and subsoil material*

Air-dried Toyoura sand, having e_{max} = 0.977; e_{min} = 0.605; G_s = 2.64; D_{10} = 0.11 mm and D_{50}= 0.23 mm, was pluviated through air to form the backfill and subsoil layers at a void ratio of about 0.650 (D_r=88%).

A series of plane strain compression (PSC) tests under low confining pressure of 9.8 kPa, which were performed on the same batch of Toyoura sand prepared at the same density, revealed that its peak and residual angles of internal friction ϕ_{peak} and ϕ_{res} were 51 and 43 degrees, respectively.

After finishing the pluviation of sand, the surface of the backfill was trimmed to the prescribed geometry, and a surcharge of 1 kPa was applied by placing lead shots on the surface of the backfill to simulate such a structure as the railway ballast fill. To separate sand from the lead shots, 0.2 mm-thick rubber membranes were placed between them.

2.3 *Application of seismic loads*

Seismic loads were applied by shaking the sand box horizontally with an irregular or a sinusoidal base acceleration. The irregular base acceleration was prepared based on a strong motion that was recorded as N-S component at Kobe Marine Meteorological Observation Station during the 1995 Hyogoken-Nanbu earthquake (refer to Fig. 4 of Watanabe et al., 2001). About 50 cycles of sinusoidal waves at a frequency of 5Hz were employed as the sinusoidal base acceleration. Each model was subjected to several shaking steps, where the maximum amplitude of the base acceleration was increased stepwise at a prescribed increment.

Results from these shaking tests were compared with those from tiliting tests, where seismic loads were applied by tilting the whole sand box at a rate of approximately 1.0 degree/minute to simulate pseudo-static loading conditions. Based on the pseudo-static approach, the observed seismic coefficient k_h in the tilting tests was defined as;

$$k_h = \tan\theta \qquad (1)$$

where θ is the tilting angle of the sand box. On the other hand, the observed seismic coefficient k_h in the shaking table tests was defined as;

$$k_h = a_{max}/g \qquad (2)$$

where a_{max} is the single amplitude of maximum base acceleration at the active state (i.e., when the inertia force of the backfill is acting outward) for each shaking step, and g is the gravitational acceleration.

3 TEST RESULTS AND DISCUSSIONS

3.1 *Residual displacement of wall*

Relationships between the seismic coefficient k_h and the horizontal displacement d_{top} measured at a distance of 5 cm below the top of the wall are shown in Fig. 2. For the shaking tests, the values of d_{top} at the end of each shaking step are plotted. In the sinusoidal shaking tests as well as the tilting tests, after exceeding about 25 mm, which corresponds to about

5% of the total wall height, the d_{top} value increased very rapidly, soon resulting into the ultimate overall wall failure.

In the early steps of irregular shaking tests up to the k_h value of about 0.5, the d_{top} value accumulated in a similar manner among different types of RWs. When the k_h value exceeded about 0.5, however, the rate of increase in the d_{top} value became larger for the three conventional type RWs than for the three reinforced-soil type RWs. Such different extents of ductility that depend on the RW type are discussed elsewhere (Watanabe et al., 2001).

3.2 *Resultant force of normal earth pressures*

Relationships between the resultant force P_a acting normally on the facing from the backfill and the seismic coefficient k_h are shown in Fig. 3. The P_a values are evaluated by integrating normal stresses measured with loadcells along depth of the facing, which include initial values measured before the start of shaking or tilting. For each irregular or sinusoidal shaking step, the P_a value was defined under three different conditions; i.e., when either one of the P_a value itself, the wall top displacement d_{top}, or base acceleration (on the negative side, inducing outward inertia force) becomes respective peak state. The k_h values are evaluated based on Eqs. (1) and (2). Note that for the tilting tests, the measured values of the normal stresses at tilted conditions were corrected for the effects of the sand box inclination by a factor of $1/(\cos\theta)$, where θ is the tilting angle.

In Figs. 3a through 3c, theoretical relationships based on the Mononobe-Okabe method are shown, while in Figs. 3d through 3f, those based on limit-equilibrium stability analysis assuming a two-wedge failure mechanism (Horii et al., 1994) are presented. In obtaining these relationships, the shear resistance angle ϕ of the backfill was set equal to ϕ_{peak} (=51 degrees), and the frictional angle δ at the interface between the backfill and the wall facing with sand paper was set equal to $3/4\phi_{peak}$ (Koseki et al., 1998a). For comparison, the residual condition of $\phi=\phi_{res}$ (=43 degrees) and $\delta = 3/4\phi_{res}$ was also employed in the calculation.

For the cantilever type RW, the resultant forces measured at the backface of the wall cannot be directly compared to the calculated values, because the calculated resultant forces are those acting on the vertical failure plane in the backfill, which was actually observed to develop from the heel of the wall base. Therefore, the resultant force P_a acting on this vertical failure plane was estimated from the measured values of the normal force P_{al} acting on the backface of the facing and the shear force T acting on the top of the wall base from the backfill as:

$$P_a = P_{al} + T - k_{hl} \times W \qquad (3)$$

where $k_{hl} \times W$ is the horizontal inertia of the soil block located above the wall base and separated by the vertical failure plane from the remaining part of the backfill (i.e., W is the weight of this soil block, and k_{hl} is the measured horizontal response acceleration a_h of this soil block divided by the gravitational acceleration g for the shaking table tests); T and $k_{hl} \times W$ are defined positive when they act in the direction toward the facing (i.e., at the active state). In this case, theoretical relationships with $\phi = \delta = \phi_{peak}$ and $\phi = \delta = \phi_{res}$ are added to the figure, since the frictional angle δ at the vertical failure plane can be assumed equal to ϕ.

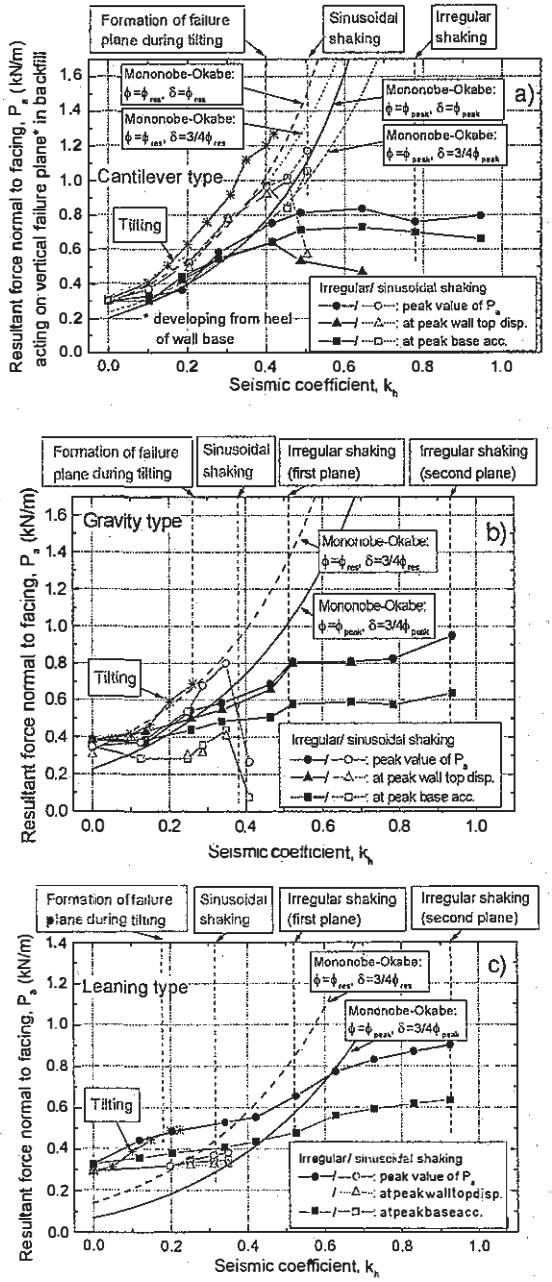

Figure 3. Relationships between resultant normal force and seismic coefficient.

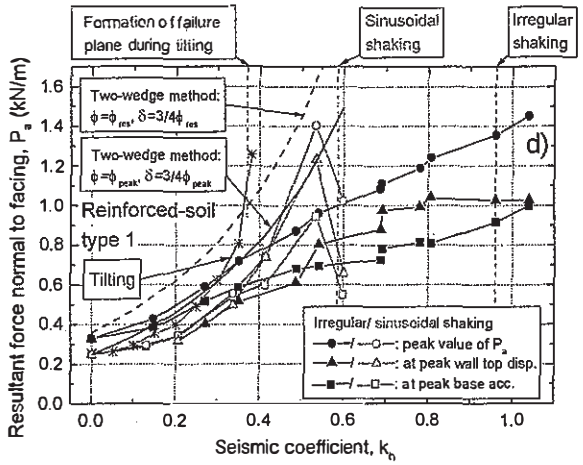

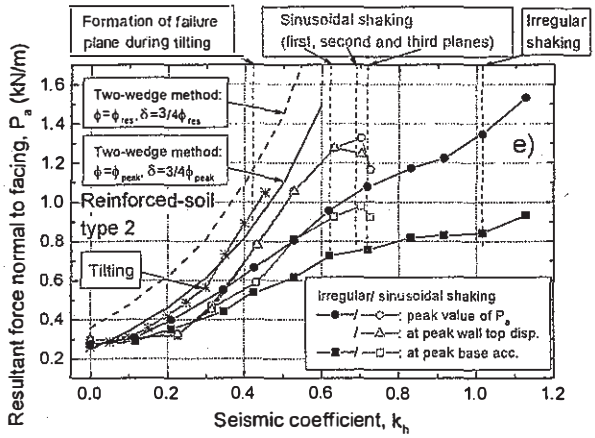

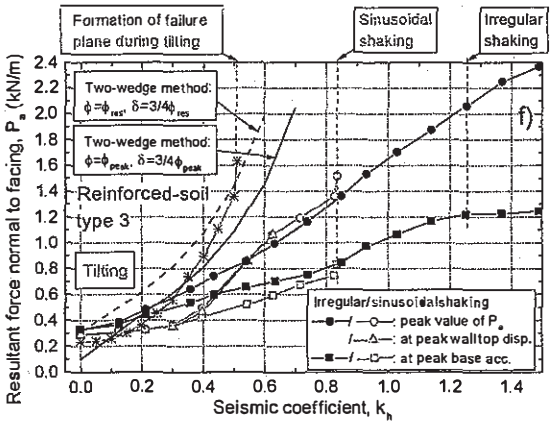

Figure 3. (continued) Relationships between resultant normal force and seismic coefficient.

It can be seen from Fig. 3 that, in general, the P_a values measured in the tilting tests were larger than those measured in the sinusoidal or irregular shaking tests. In a broad sense, the results from tilting tests were comparable with the theoretical ones, except for the leaning type RW. It should be noted, however, that the direct comparison of the measured values with those calculated by the Mononobe-Okabe or its equivalent method, be valid at the active failure state in the backfill. The active failure state could be defined as the state either when the failure plane is about to develop (for $\phi = \phi_{peak}$), or after the failure plane has developed in the backfill, where the ϕ values has dropped to ϕ_{res}.

Phase difference in the shaking tests in the vertical distribution of horizontal response accelerations of backfill would be one of the reasons for the different P_a values from the tilting tests. In addition, as discussed by Tatsuoka et al. (1998), different from the case of tilting tests, the earth pressure acting on the back of the facing in the shaking tests is controlled largely by an interaction between dynamic response of the backfill and the wall structure. In fact, the P_a values defined under the three different conditions as mentioned above were, in general, different from each other.

In Fig. 4, the peak horizontal response acceleration $(a_h)_{max}$ in the backfill inducing outward inertia force was compared with the peak base acceleration a_{max} in the irregular shaking tests. The $(a_h)_{max}$ values were evaluated based on the records of an accelerometer located near the mass center of the soil wedge (in the unreinforced zone for reinforced-soil RWs) above the failure plane. With the increase in the shaking level, the $(a_h)_{max}$ value became gradually smaller than the a_{max} value. In particular, after the failure plane was formed in the backfill, the rate of increase in the $(a_h)_{max}$ value was significantly reduced, or even the increase stopped temporarily, due possibly to sliding of the soil wedge along the failure plane.

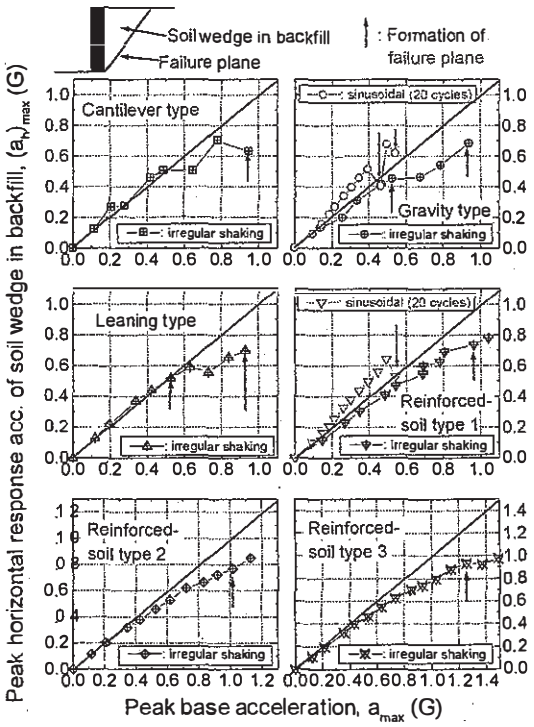

Figure 4. Relationships between peak horizontal response acceleration in backfill and base acceleration.

For gravity type and reinforced-soil type 1 RWs, results from sinusoidal shaking tests are also shown in Fig. 4. Note that, using 20 cycles of sinusoidal waves, these shaking tests were additionally conducted on limited types of RWs. In these tests, a noticeable amplification of the response acceleration took place before the formation of the failure plane, in contrast to the attenuation in the response observed in the irregular shaking tests. On the other hand, after the formation of the failure plane, a sudden reduction in the response acceleration took place in the sinusoidal shaking tests, which may also be due to sliding of the soil wedge along the failure plane.

It should also be noted that, the horizontal response of the soil wedge above the failure plane was accompanied by its vertical response, as typically shown in Fig. 5. In this case, the first failure plane had been already formed in the backfill during the previous shaking steps, and several large cycles of horizontal base acceleration induced relatively large response of the soil wedge not only in the horizontal but also in the vertical directions. The peak horizontal response acceleration was mobilized after a certain phase lag after the peak base acceleration, and, as mentioned above, the $(a_h)_{max}$ value was smaller than the a_{max} value. When outward inertia force was acting on the soil wedge, it was also subjected to vertical upward inertia force (i.e., downward acceleration) in the beginning, which was reversed into the downward inertia force (i.e., upward acceleration) in the later stage.

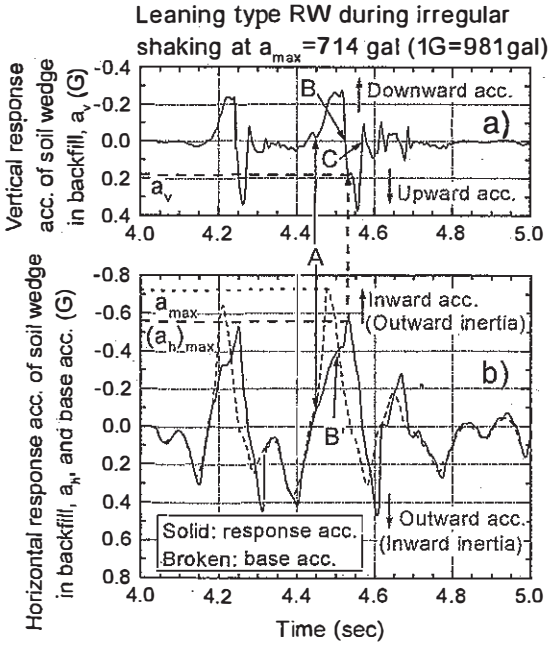

Figure 5. Typical response acceleration of soil wedge above failure plane for leaning type RW.

This peculiar behavior could be explained qualitatively by considering the sliding of the soil wedge along the failure plane as follows:

1) The broken curve in Fig. 5b is the base acceleration. When the soil wedge started sliding (after point A in Fig. 5), its horizontal response acceleration became smaller than the base acceleration. At the same time, it slid down along the failure plane with negative (downward) vertical acceleration (between points A and B in Fig. 5a).
2) Since reversal of the base acceleration took place, the sliding of the soil wedge was terminated eventually (at point C in Fig. 5a). Before the termination, the sliding movement was decelerated with positive (upward) vertical acceleration (between points B and C in Fig. 5a).
3) The point B' in Fig. 5b is the point after which the horizontal response acceleration of the soil wedge became larger than the base acceleration (i.e., when the relative horizontal acceleration of the soil wedge to the base was reversed). It was slightly different from point B (when the vertical acceleration of the soil wedge was reversed) in Fig. 5a, due possibly to that the horizontal response acceleration in the underlying non-sliding soil mass was not equal to the base acceleration. Similarly, the point that corresponds to point C in Fig. 5a (after which the horizontal response acceleration of the soil wedge became equal to the base acceleration) could not be clearly defined in Fig. 5b.

In Fig. 5, the peak horizontal response acceleration was mobilized while the sliding movement was decelerated (between points B and C). In some of the other cases, however, the peak horizontal response acceleration was mobilized while the sliding movement was accelerated (between points A and B).

In Fig. 6, correction for the effects of horizontal and vertical responses of the soil wedge during the irregular shaking was made for some RW models on the seismic coefficient k_h and the measured resultant force P_a, respectively. The k_h value was evaluated from the $(a_h)_{max}$ value. The P_a value was obtained at the moment when $(a_h)_{max}$ was mobilized, and it was corrected by dividing with a factor of "$1+a_v/g$", where a_v is the vertical acceleration of the soil wedge obtained at the same moment as above (defined as positive when it induces downward inertia force). The corrected relationships are represented by using open symbols in Fig. 6. For reference, measured relationships between uncorrected k_h and P_a values that were obtained at the moment when the base acceleration became its peak (i.e., when a_{max} was mobilized) are plotted by using solid symbols, and the aforementioned theoretical relationships are also shown. It can be seen that, by making a correc-

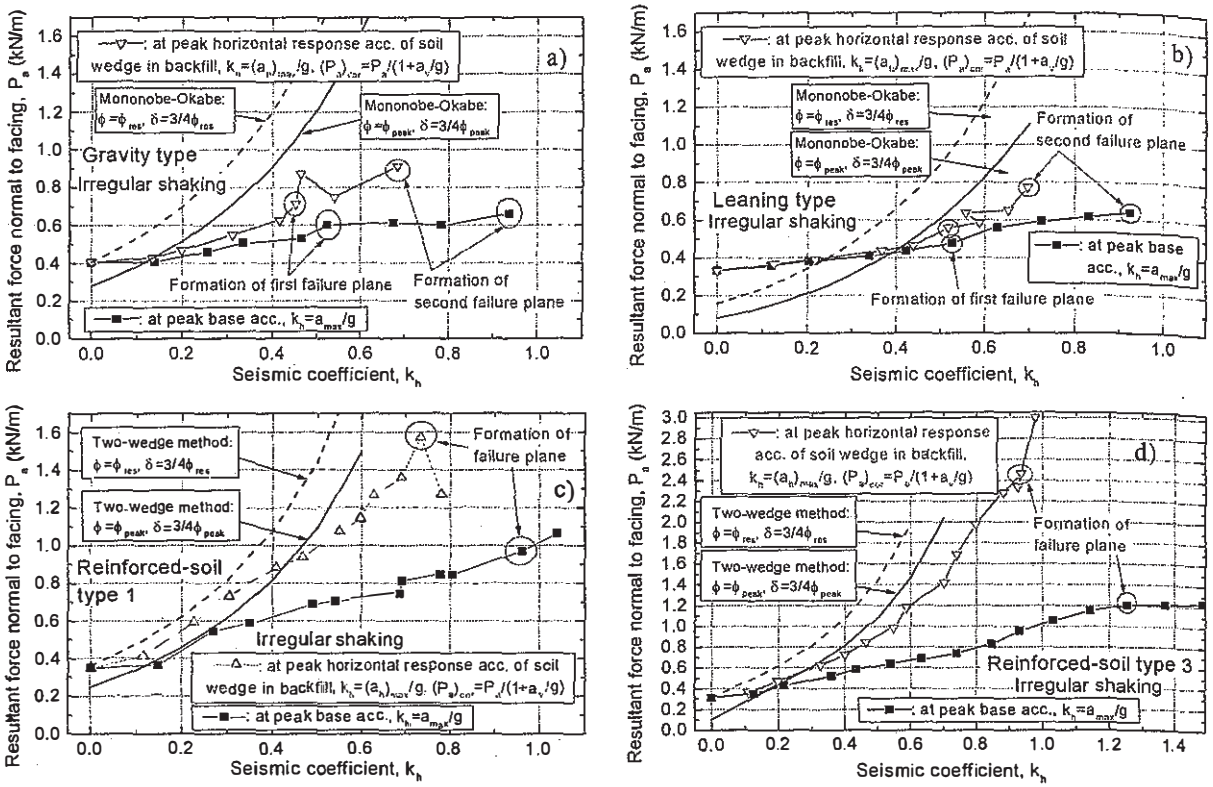

Figure 6. Effects of correction for response of soil wedge on relationships between resultant normal force and seismic coefficient.

tion to the response of the soil wedge, the measured relationships became much closer to the theoretical ones, in particular, in the region at high seismic loads.

In summary, the experimental data supports the overall trend of the Mononobe-Okabe method. In addition, sudden increase in the corrected P_a values after formation of the first failure plane as shown in Figs. 6a, 6b and 6d can be explained by the modified Mononobe-Okabe method as proposed by Koseki et al. (1998b), considering the effects of strain softening and strain localization. However, the detailed quantitative evaluation of the original or modified Mononobe-Okabe method was not possible, because of the delicate nature of dynamic earth pressures. It is readily seen that the reinforced-soil RWs could stand without exhibiting ultimate failure against earth pressures that were much higher than those acting on the conventional type RWs.

4 CONCLUSIONS

The resultant forces of normal earth pressures measured in the tilting tests were, in a broad sense, comparable with theoretical ones based on the Mononobe-Okabe or its equivalent method. On the other hand, the resultant forces measured in the sinusoidal and irregular shaking tests were smaller than those measured in the tilting tests. However, by making corrections for the horizontal and vertical response accelerations of soil wedge in the backfill, the measured values became much closed to the theoretical ones, in particular, in the region at high seismic loads.

REFERENCES

Horii,K., Kishida,H., Tateyama,M. and Tatsuoka,F. 1994. Computerized design method for geosynthetic-reinforced soil retaining walls for railway embankments, *Recent Case Histories of Permanent Geosynthetic-Reinforced Soil Retaining Walls*, Balkema: 205-218.

Koseki,J., Munaf,Y., Tatsuoka,F., Tateyama,M., Kojima,K. and Sato,T. 1998a. Shaking table and tilt table tests of geosynthetic-reinforced soil and conventional retaining wall, *Geosynthetics International*, Vol. 5, Nos. 1-2: 73-96.

Koseki,J., Tatsuoka,F., Munaf,Y., Tateyama,M., and Kojima,K. 1998b. A modified procedure to evaluate active earth pressure at high seismic loads, *Soils and Foundations*, Special Issue, No. 2: 209-216.

Koseki,J., Munaf,Y., Tateyama,M., Kojima,K. and Horii,K. 1999. Back analyses of case histories and model tests on seismic stability of retaining walls, *11th Asian Regional Conf. on Soil Mechanics and Geotechnical Engineering*, Vol. 1: 399-402.

Tatsuoka,F., Koseki,J., Tateyama,M., Munaf,Y., Horii,K. 1998. Seismic stability against high seismic loads of geosynthetics reinforced soil retaining structures, *6th International Conference on Geosynthetics*, Vol. 1: 103-142.

Watanabe,K., Tateyama,M., Kojima,K. and Koseki,J. 2001. Irregular shaking table tests on seismic stability of reinforced-soil retaining walls, this symposium.